A short-cut-method for the quantification of crystallization kinetics - Part 1: Method development

Erik Temmel[1], Holger Eisenschmidt[2], Heike Lorenz[1], Kai Sundmacher[1,2], Andreas Seidel-Morgenstern[1,3*]

[1]Max Planck Institute for Dynamics of Complex Technical Systems, Sandtorstr. 1, D-39106 Magdeburg, Germany

[2]Otto von Guericke University Magdeburg, Chair of Process Systems Engineering, Universitätsplatz 2, D-39106 Magdeburg, Germany

[3]Otto von Guericke University Magdeburg, Chair of Chemical Process Engineering, Universitätsplatz 2, D-39106 Magdeburg, Germany

Abstract

Population balance models are of high interest for the efficient design, control and optimization of crystallization processes. They usually contain mathematical sub-models for the description of the relevant kinetic phenomena, such as growth, dissolution and nucleation of particles. Commonly, component-specific parameters included in these sub-models have to be determined for every substance system of interest or even for the specific experimental set-up. Thus, a short-cut-method is suggested that is based on analyzing the evolution of the crystal size distribution during a few batch crystallization experiments to efficiently parameterize kinetic sub-models required to predict and evaluate the performance of crystallization processes. To illustrate the overall procedure and to evaluate the accuracy of the proposed approach, in silico data with pre-defined kinetics corresponding to hypothetical non-isothermal batch runs are analyzed. It is shown that it is possible to recover pre-specified sub-model parameters with a rather limited amount of input information. Subsequently, less flexible sub-models and measurement errors are considered for comparison, in order to evaluate the loss of predictability. The agreement found between the results of a simulated continuous crystallization process applying both, (a) the initially provided model together with the pre-specified parameters or (b) parameter estimates provided by the short-cut-method demonstrates the practical applicability of the latter.

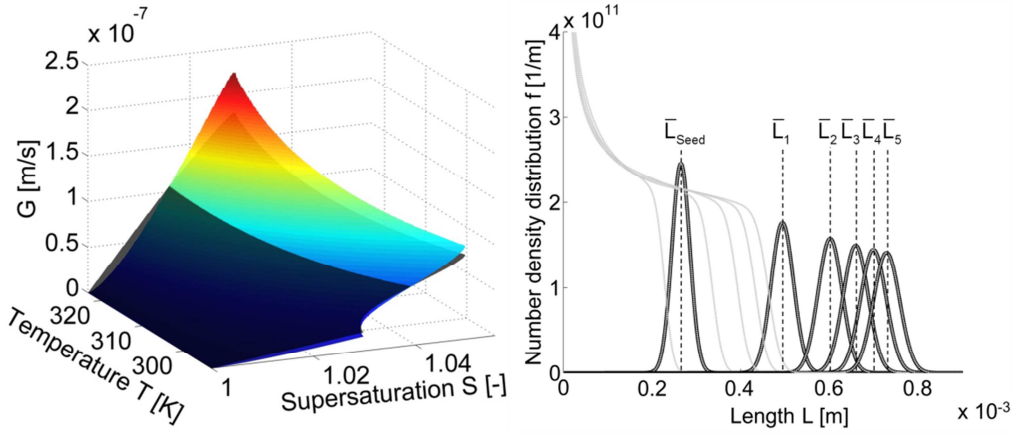

Corresponding author: Andreas Seidel-Morgenstern
Max Planck Institute for Dynamics of Complex Technical Systems; Sandtorstraße 1, 39106 Magdeburg, Germany
Tel: +49 391 6110401; Fax: +49 391 6110521
Email: seidel@mpi-magdeburg.mpg.de

A short-cut-method for the quantification of crystallization kinetics - Part 1: Method development

Erik Temmel[1], Holger Eisenschmidt[2], Heike Lorenz[1], Kai Sundmacher[1,2], Andreas Seidel-Morgenstern[1,3*]

[1]Max Planck Institute for Dynamics of Complex Technical Systems, Sandtorstr. 1, D-39106 Magdeburg, Germany

[2]Otto von Guericke University Magdeburg, Chair of Process Systems Engineering, Universitätsplatz 2, D-39106 Magdeburg, Germany

[3]Otto von Guericke University Magdeburg, Chair of Chemical Process Engineering, Universitätsplatz 2, D-39106 Magdeburg, Germany

* Corresponding author: seidel@mpi-magdeburg.mpg.de

Abstract

Population balance models are of high interest for the efficient design, control and optimization of crystallization processes. They usually contain mathematical sub-models for the description of the relevant kinetic phenomena, such as growth, dissolution and nucleation of particles. Commonly, component-specific parameters included in these sub-models have to be determined for every substance system of interest or even for the specific experimental set-up.

Thus, a short-cut-method is suggested that is based on analyzing the evolution of the crystal size distribution during a few batch crystallization experiments to efficiently parameterize kinetic sub-models required to predict and evaluate the performance of crystallization processes. To illustrate the overall procedure and to evaluate the accuracy of the proposed approach, in silico data with pre-defined kinetics corresponding to hypothetical non-isothermal batch runs are analyzed. It is shown that it is possible to recover pre-specified sub-model parameters with a rather limited amount of input information. Subsequently, less flexible sub-models and measurement errors are considered for comparison, in order to evaluate the loss of predictability. The agreement found between the results of a simulated continuous crystallization process applying both, (a) the initially provided model together with the pre-specified parameters or (b) parameter estimates provided by the short-cut-method demonstrates the practical applicability of the latter.

Keywords: Crystallization processes, Particle size distributions, Kinetics, Nucleation, Growth, Dissolution

1. Introduction

Many industrially important substances are produced with a tailored product quality via crystallization. Ordinary sugar, for example, is desired to have a narrow crystal size distribution (CSD) with a mean value of 700-800 µm, almost without fine material and a

purity of 99.5% [1]. This is feasible exploiting one single seeded batch process based on the experience accumulated over many decades. For current industrial applications, faster approaches are needed to design crystallization processes. Increasingly theoretical concepts based on population balance equations (PBE) are utilized for this purpose. However, it is difficult to quantify the corresponding rates, e.g. for growth, nucleation and dissolution, which are required for this mathematical framework [2].
Several publications describe a rather simple method, based on the observation of the evolution of the solid and liquid phase during well planned cooling batch crystallization in order to quantify the necessary crystallization kinetics. Obviously, crystal populations move to larger particle sizes due to growth (*G*) and to smaller sizes due to dissolution (D) (Fig. 1a and 1b, [3, 4]). It was theoretically shown, e.g. in [5], that it is possible to determine the growth rate by evaluating one specific characteristic of the CSD during crystallization.
Hence, it is straightforward to exploit seeded batch crystallization experiments for this purpose if size-independent growth [6] is assumed even though growth rate dispersion occurs. The crystals, which are initially provided with an appropriate size and shape, can be observed during the crystallization process utilizing suitable online or offline measurement techniques, as e.g. sieve analysis or online microscopy. Therefore, the seed particles should be large enough to distinguish them from eventually occurring nuclei and the substance-specific crystal shape should be developed completely to reduce their agglomeration tendency. Based on their specific growth or dissolution rates, the crystals move during the process with a certain velocity through the space of the characteristic coordinates (e.g. length or width of the particles). Thus, it is instructive and valuable to quantify the crystal size evolutions since they contain information regarding the underlying growth or dissolution kinetics. This information can be utilized directly (without the need of solving full population balance equations, PBE) together with observed supersaturation and temperature in the crystallizer to estimate free parameters in postulated kinetic sub-models for growth or dissolution.
A similar simple procedure can be applied to analyze observed appearance (birth) rates of new crystals (B_0). Observed positive temporal changes in the total number of crystals (*N(t)*, Fig. 1c), are directly connected to the nucleation kinetics provided that breakage and agglomeration events are negligible.

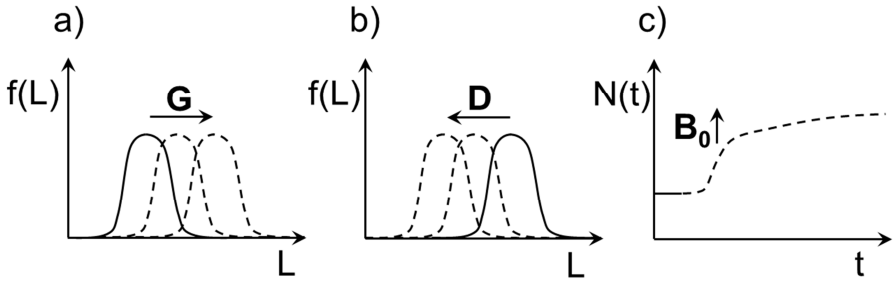

Fig. 1: *a) & b):* Movement of a seed-peak due to crystal growth (*G*) and dissolution (*D*). *c):* Change of the particle number (*N(t)*) of the CSD due to nucleation (B_0) [7]. *Solid lines:* Initial state; *Dashed lines:* Evolution of the state.

Altogether, the described evaluation procedure based on classical experiments leads to an efficient and fast quantification scheme. Essential information is extracted from measured CSDs and applied directly for the parameterization of different postulated kinetic models. The just described simple ("PBE-free") procedure will be designated in the following as "Short-cut-method".
In recent years, several authors performed investigations around this main idea. One work describes the experimental set-up and data processing to calculate nucleation and growth rates during seeded cooling crystallizations at fixed supersaturation [8]. In that work, laser diffraction was applied to investigate the solid phase that can lead to errors when the crystal shape differs significantly from perfect spheres since reflections of facetted particles and the orientation of crystals influence the result significantly [9, 10]. Furthermore, the mean length of the whole crystal size distribution (CSD) was taken as an indicator for the growth of the particles [8]. This eventually obscures the real growth rate, in particular if nucleation occurs.
Yokota et al. [11] analyzed four precisely determined CSDs of one non-isothermal batch crystallization and identified successfully the three parameters ($k_{g,0}$, $E_{A,g}$, g) of an assumed temperature-dependent power law for the crystal growth kinetics (eq. 1)

$$G = k_{g,0} \exp\left(\frac{-E_{A,g}}{RT}\right)(S-1)^{g} \qquad \text{(eq. 1)}$$

It is however rather difficult to accurately measure CSDs during an experiment. Consequently, four determined crystal size distributions may not be sufficient.
In this paper, the potential of the short-cut-method is investigated more systematically utilizing predicted transients of batch experiments. The approach of [11] is extended in order to identify besides growth, also nucleation and dissolution kinetics and to evaluate the impact of the number, type and precision of input data on the quality of the estimated kinetic parameters.
It is shown, that only a few experiments are necessary to estimate all basic crystallization kinetics for a large range of supersaturation and temperature. Furthermore, the numerical effort is reduced since no full PBE model is applied and only the parameters of one postulated kinetic sub-model is quantified at once.
Finally the applicability of the short-cut method is also tested by comparing design scenarios for a continuous crystallization process using various parameter constellations.
This article is organized as follows: In the following section, the model framework that was applied for the generation of synthetic ("perfect") crystallization data is explained together with the properties of the assumed substance system. Subsequently, a synthetic reference data set of crystallization experiments is created. In the third section, the short-cut-method is explained in detail and the analysis of the synthetic crystallization experiments is presented. In the fourth section, the parameter optimization is shown for different amounts of data with and without noisy measurement signals. In the last section, a continuous crystallization process is designed with the estimated kinetic rates and with the initially provided values for comparison. Finally, all results are evaluated in a concluding section.

2. Generation of *in silico* process data

For the evaluation of the short-cut-method, *in silico* data of batch crystallization experiments are generated and subsequently analyzed. A one-dimensional PBE system is used to create the required information. This ideal case assumes (at first) perfect concentration and temperature signals as well as a highly accurate measurement of the size distribution during the experiment. The model framework and all necessary process and kinetic parameters are explained in the following.

2.1. Model framework

For the crystallization case, the general population balance reduces to equation 2 if breakage and agglomeration are neglected, size independent growth and ideal mixing without volume contraction due to an occurring solid phase are assumed [12].

$$\frac{\partial f(t,L)}{\partial t} = -G(S(t),T(t))\frac{\partial f(t,L)}{\partial L} \qquad \text{for S} \geq 1 \qquad \text{(eq. 2)}$$

Here, L is the internal size coordinate and G represents the growth rate. The corresponding driving force for crystal growth in equation 2, is the supersaturation, which is defined for ideal solutions [13] as the ratio between the actual concentration, c, and the saturation concentration, $c^*(T)$, at a certain saturation temperature.

$$S = \frac{c}{c^*(T)} \qquad \text{(eq. 3)}$$

For the simple batch case, the corresponding mass balance consists of the accumulation in the liquid phase and the transport of substance to the solid phase due to crystallization.

$$\frac{dc(t)}{dt} = -\frac{3k_v\rho_{solid}G(S(t),T(t))}{V_{solvent}\rho_{solvent}}\int_{L\min}^{L\max} L^2 f(t,L)dL \qquad \text{(eq. 4)}$$

It should be noted that a constant solvent mass is assumed in equation 4. The population balance was subsequently discretized applying a finite volume method together with the upwind scheme [14], since an analytical solution is not available for this PDE system.

For the resulting ODE system, three initial conditions (IC) are required. It is assumed that the seed crystals can be characterized by a perfect Gaussian distribution (eq. 5) with a certain mean value, $\overline{L}_{Seed}$, and standard deviation, σ_{Seed}. Even though the same seed mass is used throughout the simulations, the initial distribution is scaled to a certain mass, m_{Seed}, with equation 6 since the Gaussian distribution is normalized.

$$f_{0,Seed}(L) = \frac{1}{\sigma_{Seed}\sqrt{2\pi}} \exp\left(-\frac{1}{2}\left(\frac{L-\bar{L}_{Seed}}{\sigma_{Seed}}\right)^2\right) \quad \text{(eq. 5)}$$

$$f_{Seed}(L) = f_{0,Seed}(L) \cdot \frac{m_{seed}}{k_v \rho_{solid} \int_{L\min}^{L\max} L^3 f_{0,Seed}(L) dL} \quad \text{(eq. 6)}$$

Furthermore, it is assumed that the liquid phase is saturated at a certain temperature, T_0, with a concentration c^0 (eq. 8). The occurrence of new crystals due to nucleation is introduced as an initial condition at the crystal size $L = 0$ (eq. 9). Subsequently, all conditions are defined for the crystallization case as follows:

IC for S > 1:

$$f(t=0,L) = f_{Seed}(L) \quad \text{(eq. 7)}$$

$$c(t=0) = c^0 = c^*(T_0) \quad \text{(eq. 8)}$$

$$f(t,L=0) = \frac{B_0}{G} \quad \text{(eq. 9)}$$

Similar to [11] (eq. 1), temperature and supersaturation dependent power-law approaches with three parameters (eq. 10) are applied to quantify the rates of the specific phenomena considered in equations 2, 4 and 9.

$$K = p_1 \exp\left(\frac{-p_2}{RT}\right)(S-1)^{p_3} \qquad \text{for K = G, D, } B_0 \quad \text{(eq. 10)}$$

Here, p_1 is the pre-exponential factor, k_0, p_2 is usually referred to as the activation energy, E_A, and p_3 is the power law exponent.
The *in silico* batch crystallization experiments were predicted as a combination of crystallization and dissolution to have information about all three kinetic phenomena considered in this study within one experiment.
At first, after seeding the crystallizer is cooled down linearly until a certain temperature difference is achieved. Hence, the driving force will raise and nucleation and growth of present crystals will take place. Subsequently, the reactor is heated again with a linear temperature ramp back to the starting temperature. The dissolution rate, D, replaces the growth rate, G, in equations 2, 4 and 9 in case of undersaturation (S<1). Furthermore, the initial conditions (eqs. 7-9) have to be adjusted properly in the model frame work. In particular, particles approaching size zero have to vanish from the overall population. Hence, individuals leaving the first element of the finite volume grid due to dissolution are erased from the entity.
The whole model (eqs. 2-9) was implemented in Matlab and the solutions were obtained via time integration using a Runge-Kutta method of 4th order [15]. All hypothetical

experiments were calculated for time steps of 10 s and 2000 finite volume elements of the internal coordinate to have moderate numerical diffusion at reasonable computational costs. The crystal size coordinate was discretized equidistantly between 1 µm and 2 mm.
All necessary kinetic parameters and the process conditions are given in the subsequent section.

2.2. Model parameters and simulated experimental data

For the simulation of the process data with the model framework introduced before, substance characteristics are required such as the solubility, the physical properties and parameters for the kinetics. Potassium alum is chosen in the present study as a model substance since it is a well-known compound for which the needed data is easily accessible. The solubility curve measured in preliminary experiments was approximated with a 4th order polynomial (eq. 14) and fitted to own experimental results (Fig. 2).
Simulations of process trajectories with the PBE model requires compound specific characteristics such as physical properties, the solubility and rate laws including the parameters for the kinetics of the considered sub-processes. Parameters corresponding closely to the well-studied compound potassium aluminum sulfate dodecahydrate (potassium alum) were selected in the present study. The solubility curve measured in own preliminary experiments [7] was expressed using a 4th order polynomial (eq. 14, Fig. 2).

$$c^* = p_{S,1} + p_{S,2}\theta + p_{S,3}\theta^2 + p_{S,4}\theta^3 + p_{S,5}\theta^4 \qquad \text{(eq. 14)}$$

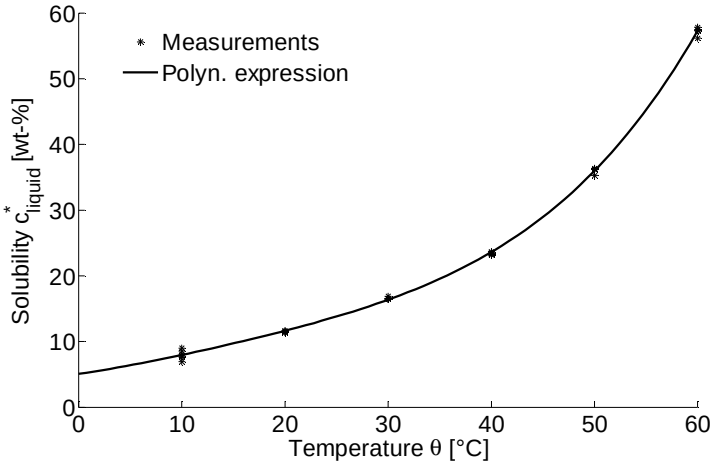

Fig. 2: Solubility curve of potassium aluminum sulfate dodecahydrate. Stars depict solubility measurements and the bold line illustrates the description applying a 4th order polynomial (eq. 14).

It should be mentioned, that errors of the solubility measurements and the corresponding mathematical expression can be a major source for erroneous parameter estimates. Therefore, this error influence is discussed in detail in section 4.2.

The physical characteristics of the solid phase as well as the solubility parameters, $p_{S,i}$, are given in Table 1. The solid density corresponds to the value in [13] and the volume shape factor describes a perfect octahedron, which is the typical crystal shape of potassium alum grown from water.

Table 1: Physical properties and solubility parameters of potassium alum.

	Symbol	Value	Unit
Solid density [13]	ρ_{solid}	1750	[kg/m^3]
Volume shape factor	k_V	$\sqrt{2}/3$	[-]
Solub. Parameter 1	$p_{S,1}$	5.06	[wt-%]
Solub. Parameter 2	$p_{S,2}$	0.23	[wt-%/°C]
Solub. Parameter 3	$p_{S,3}$	7.76×10^{-3}	[wt-%/°C^2]
Solub. Parameter 4	$p_{S,4}$	-2.43×10^{-4}	[wt-%/°C^3]
Solub. Parameter 5	$p_{S,5}$	4.86×10^{-6}	[wt-%/°C^4]

Several authors investigated the crystallization kinetics of potassium alum over the past decades either with empirical approaches [11, 16] or based on thermodynamics [17]. In this article, kinetic equations and parameters are applied related to results of the mentioned own preliminary experimentally studies applying the short-cut-method analyzed here in more detail [7]. The parameter of the assumed power law sub-models (eq. 10) are listed in table 2. They were utilized to describe growth, nucleation or dissolution within the PBE model to generate transients of *in silico* batch experiments.

Table 2: Provided kinetic parameters of the pre-specified rate laws (eq. 10) for growth, nucleation and dissolution to be recovered by the short-cut-method. p_1 - pre-exponential factor, k_0; p_2 - activation energy, E_A; p_3 - exponent.

Kinetic	$\mathbf{p_1}$ [m/s; 1/s]	$\mathbf{p_2}$ [J/mol]	$\mathbf{p_3}$ [-]
Growth G	5×10^7	75×10^3	1.4
Nucleation B_0	1×10^{15}	50×10^3	1.5
Dissolution D	6.5×10^{-6}	100	1.1

To predict *in silico* transients it was assumed that the processes of interest occur in a temperature range between 293 K to 323 K. In accordance to the preliminary studies, three different starting points with respect to the initial temperature of the batch runs were chosen, namely 303 K, 313 K and 323 K, in order to cover a significant range of supersaturation.
All three simulations of seeded batch runs started from solutions saturated at the just mentioned initial temperatures. With respect to modulated temperature changes, simple linear cooling ramps were considered. In this case study, the cooling rates were fixed at

-5 K/h. This provided sufficient supersaturation, required for the identification of the kinetic parameters. Higher cooling rates would lead to severe nucleation, hampering the required observation of the growth rate of the seed crystals.
Immediately after a total cooling by 10 K, in order to investigate the dissolution rate within the same run, linear heating was initiated until the initial saturation temperature was reached again. To generate an appropriate undersaturation, the heating rate was set to 20 K/h since dissolution proceeds faster than crystal growth.
The CSD of the initial seeds was assumed to have a Gaussian distribution (eq. 5) with a mean length of 265 µm and a standard deviation of 20 µm. This scenario corresponds to a sieve fraction between 150 µm and 400 µm. The initial mass of the crystal phase was adjusted in the simulations to 0.57 $g_{Seed}/kg_{Solvent}$ (5% of the expected product mass on average). Based on the available knowledge regarding the specific system [7], this ensures a good observability of the growth process while the initial crystal surface area is not strongly limiting the attainable supersaturation.
Except for the initial temperatures all assumed parameters, which are summarized in table 3, were kept constant during all experiments. The temperature, concentration and supersaturation levels for all three simulations are depicted in figure 3.

Table 3: Process conditions for the simulated batch crystallizations. All parameters were kept constant except the initial saturation temperature. Exp. 1: T_0 = 303.15 K; Exp. 2: T_0 = 313.15 K; Exp. 3: T_0 = 323.15 K.

Parameter	Value	Unit
Saturation temperature, T_0	303, 313, 323	[K]
Final temperature, T_{end}	293, 303, 313	[K]
Initial supersaturation, S_0	1	[-]
Cooling ramp	-5	[K/h]
Heating ramp	20	[K/h]
Seed mass, m_{Seed}	0.57×10^{-3}	[$kg_{Seed}/kg_{Solvent}$]
Mean seed length, $\bar{L}_{Seed}$	265	[µm]

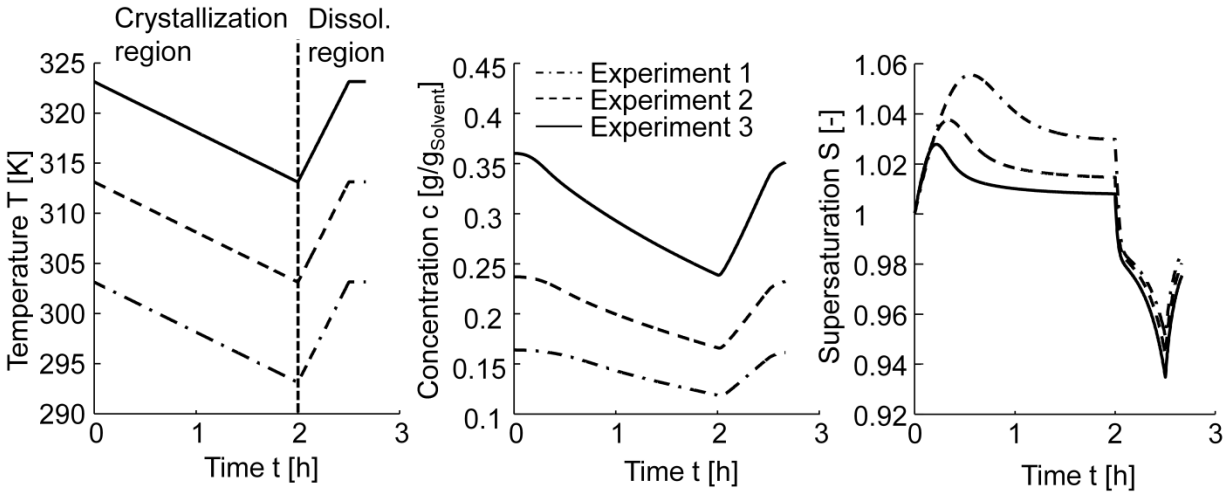

Fig. 3: Temperature, concentration and supersaturation of the simulated batch experiments. Exp. 1: T_0 = 303 K; Exp. 2: T_0 = 313 K; Exp. 3: T_0 = 323 K.

The results shown in figure 3 reveal, that all three sets of process parameters were well selected to cover reasonable ranges super- and undersaturation during the cooling and heating ramps, respectively. This selection was guided by the available *a priori* knowledge about the system considered [7]. Nevertheless, if first estimates of the crystallization kinetics exist, efficient tools [18, 19, 20] can be utilized to improve the selection of process parameters and to enhance the accuracy of the subsequent parameter optimization by setting convenient experimental conditions.

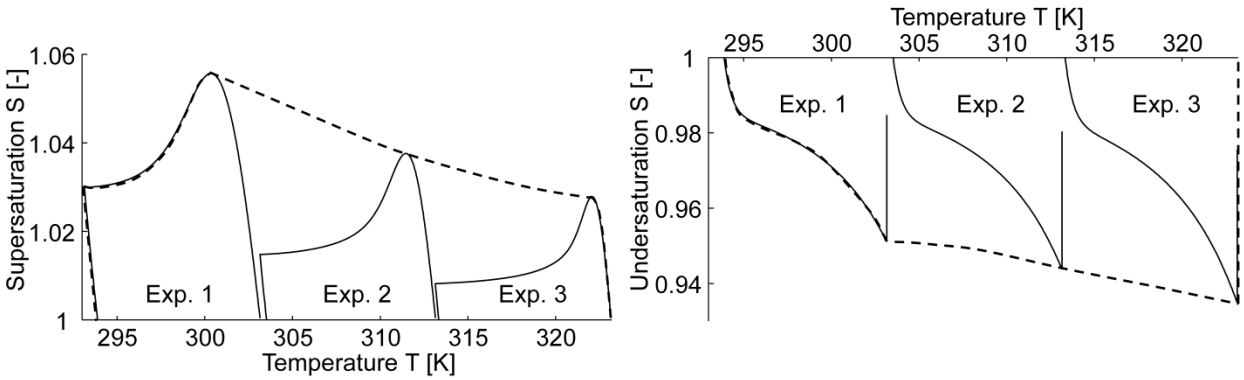

Fig. 4: Trajectories of the three in *silico batch* experiments. Dashed lines illustrate the maximum ranges of temperature and super-/ undersaturation covered, for which parameters can be estimated in corresponding rate laws.

The covered super- and under-saturation, together with the process temperatures, define the ranges, in which kinetic parameter can be estimated (Fig. 4) exploiting the available quasi-experimental data. In case of a successful fit, these ranges also limit the region of validating the rate laws.
In the following, the predicted driving forces, process temperatures and the evolutions of the solid phase as simulated for the three runs will be used to re-estimate the pre-specified parameters of the assumed corresponding kinetic laws (eq. 10) for the different sub-steps growth, dissolution and nucleation.

3. Data processing for the short-cut-method

As described, the short-cut-method is based on observations of the evolution of the particulate and continuous phases in batch experiments. Information regarding the liquid phase, i.e. supersaturation and temperature level, are applied together with transients of crystal lengths to evaluate growth and dissolution kinetics. Additionally, the nucleation kinetics can be quantified evaluating the observed changes of the particle numbers instead.
However, it is usually not possible in real processes to measure the CSD inline and continuously during the entire experiments. Therefore, a discrete sampling of the solid phase is typical and assumed here that yields only a few distinct crystal size distributions at discrete times during the process (Fig. 5 b). Subsequently, the essential information about growth dissolution and nucleation have to be extracted using only these few discrete CSDs.

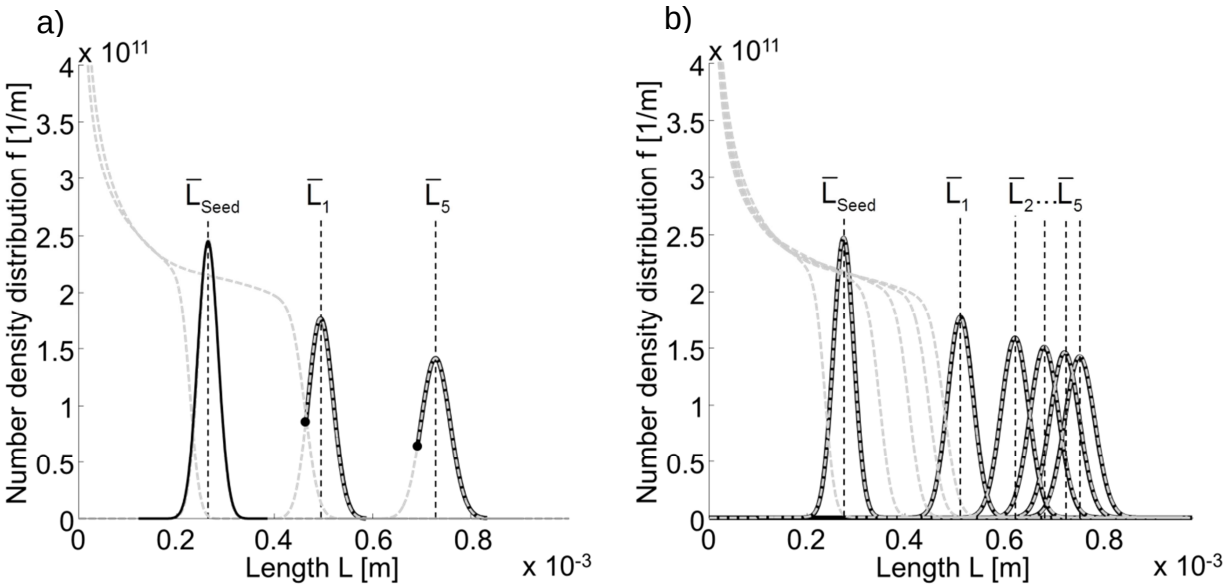

Fig. 5: *a)*: Data utilized for the parameter estimation of the Gaussian distribution exemplarily shown for sample one and five. *Dots*: smaller inflection points of the grown seed fractions; *black lines*: initial seeds and data of sample one and five utilized for the parameter estimation. *b)*: Five sampled crystal size distributions (grey dashed lines) with labeled mean lengths of the growing seed population (Exp. 3). The underlying black solid lines illustrate the Gaussian distribution fitted to the grown seed fractions.

To characterize the growth behavior it is sufficient to follow the mean length of the growing seed fraction (eq. 15).

$$\bar{L} = \frac{\int_{L_{\min}}^{L_{\max}} L f(t,L) dL}{\int_{L_{\min}}^{L_{\max}} f(t,L) dL} \qquad \text{(eq. 15)}$$

This mean length is a characteristic for the growth of the entire crystal population, which is not influenced by growth rate dispersion, if size independent growth is assumed. However, it is practically impossible to define the correct L_{min} and L_{max} that corresponds only to the growing seed fraction from an entire CSD as nucleation, breakage or agglomeration can be involved.

Nevertheless, it is assumed that the distribution function, which describes the seeds initially best, e.g. a Gaussian distribution, is conserved during the crystallization. It is then convenient, to fit the mean value and standard deviation of this function (eq. 5) using a part of the grown seed fraction (black lines indicate the utilized data for sample one and five in Fig. 5 a). In the case of simulated datasets, it is straight forward to identify this seed crystal distribution from the simulation results, as they are always the largest sub-population in the entire CSD. Classification between the seed crystal population from nucleated crystals was in this work ensured by considering only the crystal sizes that were larger than the smaller inflection point of the grown seed distribution (dots in Fig. 5 a) that was automatically detected for the parameter fitting. In case of real CSD measurements, this classification is, however, not feasible and is therefore discussed in detail in the second part of this article series. Subsequently, distortions due to nucleation (and breakage/ agglomeration for real experiments) can be attenuated by application of the estimated Gaussian distributions (black lines in Fig. 5 b) and the corresponding parameters.

After a successful fit of the distribution function to the growing seed fraction of each CSD, a set of values for the parameters $\bar{L}$ and σ is obtained. This finally yields the transient evolution of the mean length of the growing seed fraction and therefore the required objective information about the growth kinetics, $\bar{L}_{exp}(t, S, T)$. A similar procedure can be applied during the dissolution of the crystal population, to acquire the necessary information for the corresponding dissolution kinetics.

Furthermore, the measured CSDs are integrated yielding the total particle number, $N_{exp}(t, S, T)$. The increase of particles while the solution is supersaturated can be utilized for the determination of the specific nucleation sub-model (e.g. eq. 10).

The simulated data of all three experiments were sampled equidistantly 5 times while super- or under-saturation was present. Hence, small deviations with respect to time occur since the change from crystallization to dissolution differs between the experiments. The acquired CSDs were processed as described above to obtain the necessary data (Points in Fig. 6 and 7) for the subsequent parameter estimation.

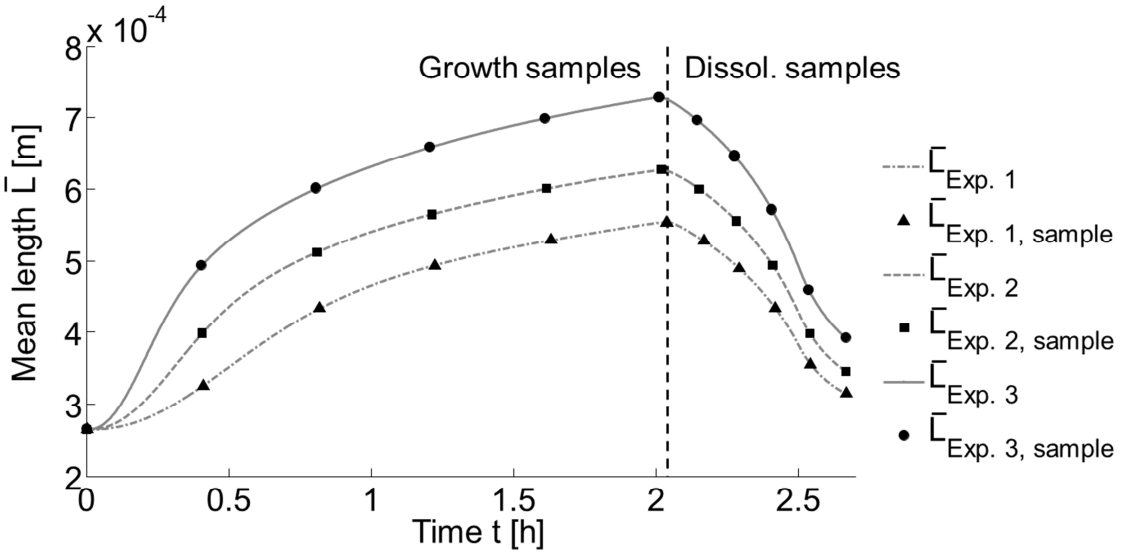

Fig. 6: Sampled mean length of the growing/ dissolving seed fraction from the size distributions, which serve as input information for the growth and dissolution parameter estimation. Points: Mean lengths of the seed fraction of the sampled CSD; Grey lines: Trends for the entire experiments.

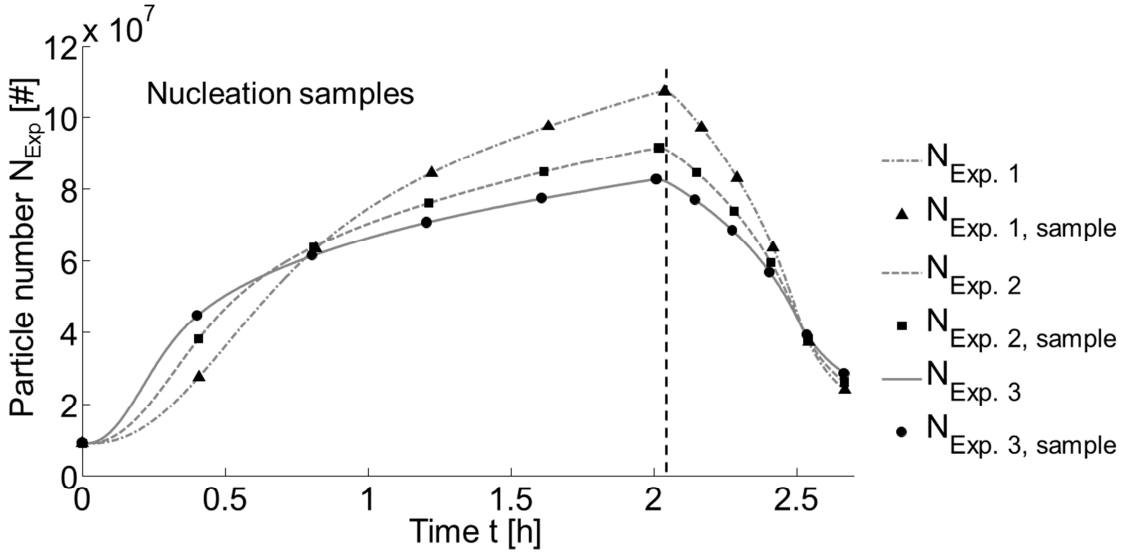

Fig. 7: Sampled particle number evolution from integrated number density distributions, which serve as input information for the nucleation parameter estimation. Points: Total particle numbers of the sampled CSD; Grey lines: Trends for the entire experiments.

4. Parameter estimation

At first, it will be shown that the kinetic parameters given in table 2 can be re-estimated with the data set discussed in section 3. The objective functions, applying a least squares method for the three experiments (n_{Exp} = 3) with five samples ($n_{Samples}$ = 5), are:

$$OF_G = \sum_{j=1}^{n_{Exp}} \sum_{i=1}^{n_{Sample}} \left(\bar{L}_{sim,i,j} - \bar{L}_{\exp,i,j} \right)^2 \qquad \text{for } S \geq 1 \qquad \text{(growth)} \qquad \text{(eq. 16)}$$

$$OF_B = \sum_{j=1}^{n_{Exp}} \sum_{i=1}^{n_{Sample}} \left(N_{sim,i,j} - N_{\exp,i,j} \right)^2 \qquad \text{for } S \geq 1 \qquad \text{(nucleation)} \qquad \text{(eq. 17)}$$

$$OF_D = \sum_{j=1}^{n_{Exp}} \sum_{i=1}^{n_{Sample}} \left(\bar{L}_{sim,i,j} - \bar{L}_{\exp,i,j} \right)^2 \qquad \text{for } S < 1 \qquad \text{(dissolution)} \qquad \text{(eq. 18)}$$

The values $\bar{L}_{sim}$ and N_{sim} in these objectives can be calculated by:

$$\bar{L}_{sim} = \bar{L}_{seed} + \int_0^t k_{g,0} \exp\left(\frac{-E_{A,g}}{RT}\right)(S-1)^g \, dt \qquad \text{for } S \geq 1 \qquad \text{(eq. 19)}$$

$$N_{Sim} = N_{Seed} + \int_0^t k_{b,0} \exp\left(\frac{-E_{A,b}}{RT}\right)(S-1)^b \, dt \qquad \text{for } S \geq 1 \qquad \text{(eq. 20)}$$

$$\bar{L}_{sim} = \bar{L}_{S<1} - \int_0^t k_{d,0} \exp\left(\frac{-E_{A,d}}{RT}\right)\left|(S-1)\right|^d \, dt \qquad \text{for } S < 1 \qquad \text{(eq. 21)}$$

where $\bar{L}_{S<1}$ stands for the last mean length of the grown seed fraction before undersaturation is established. All kinetic sub-models (eqs. 19-21) were fitted to the corresponding data separately, applying the Nelder-Mead simplex algorithm [21] with a stochastic generator for the initial guess. The range of the initial values of the different parameters was chosen based on experience. Thereby, three parameters were estimated for each mechanism separately evaluating different data sets. The obtained parameters minimizing all objective functions are summarized in table 4 (compare table 2).

Table 4: Values of the estimated kinetic parameters (eq. 10) and the corresponding average errors (eq. 23) for growth, nucleation and dissolution applying the data of 3 *in silico* experiments where 5 samples were taken. p_1 - pre-exponential factor, k_0; p_2 - activation energy, E_A; p_3 - exponent.

Kinetic	free parameters		p_1 [m/s; 1/s]	p_2 [J/mol]	p_3 [-]	$Error_{average}$ [%] (Eq. 23)
Growth G	3	Est.	4.6×10^{7}	74.8×10^{3}	1.39	0.04
		Orig.*	5×10^{7}	75×10^{3}	1.4	
Nucleation B_0	3	Est.	8.9×10^{14}	49.8×10^{3}	1.49	0.1
		Orig.*	1×10^{15}	50×10^{3}	1.5	
Dissolution D	3	Est.	5.9×10^{-6}	2.1×10^{-4}	1.11	0.16
		Orig.*	6.5×10^{-6}	100	1.1	

*Table 2

As expected, small deviations occur between the given kinetic parameters and the re-estimates even with undisturbed simulated data due to the well-known correlation between the parameters in power laws [22, 23]. Furthermore, numerical errors resulting from the discretization, the tolerances of the applied Runge-Kutta-method and the optimization routine as well as errors from the adaption of the seed-peak affect the parameter estimation.
However, the deviation of p_2 of the dissolution kinetics is conspicuous. Nevertheless, the absolute error of the activation energy of all three mechanisms is in the same range. Furthermore, the initial value of 100 J/mol for p_2 represents almost temperature independency of the dissolution kinetics. Hence, the large relative error of p_2 of this kinetics is not significant since also the deviation of the overall dissolution kinetics is very small as well (table 4, $Error_{average}$ = 0.16%).
The left hand side of figure 8 shows the corresponding logarithmic objective function for growth calculated for various pre-exponential factors and various exponents, $log(OF_G(k_{g,0},g)$. The logarithmic objective growth function calculated for different pre-exponential factors and for different activation energies, $log(OF_G(k_{g,0},E_{A,g})$, is depicted on the right side of figure 8.

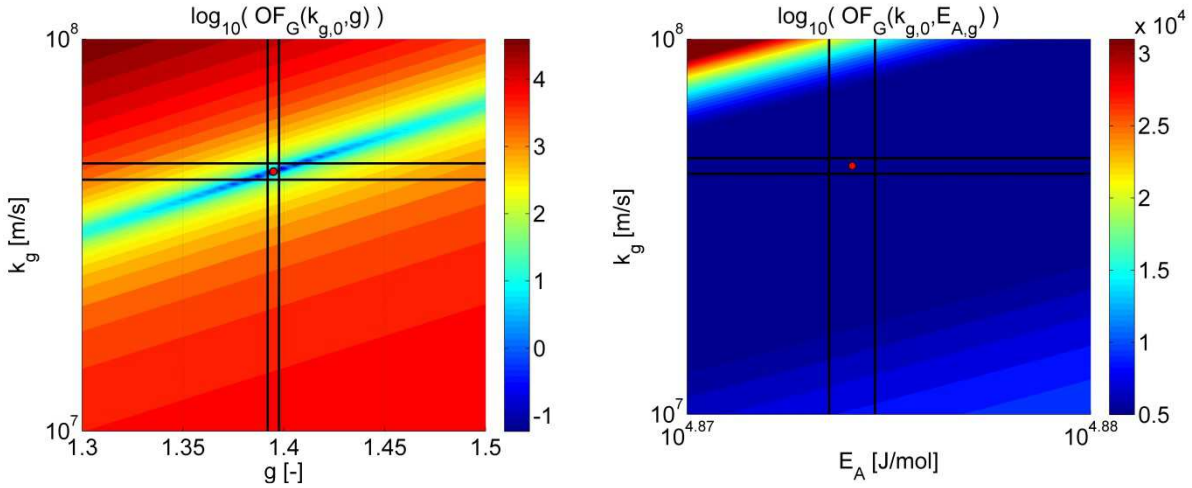

Fig. 8, *left***:** Logarithmic dependence of the objective function on the pre-exponential factor and the exponent in eq. 10 with constant estimated activation energy; *Right*: Logarithmic objective as a function of the pre-exponential factor and the activation energy of eq. 10 with constant estimated exponent (activation energy values of the abscissa are chosen to provide a good visibility of the optimum). *Bold black lines:* Individual 95% confidence intervals.

In both cases, the objective function depicts straight contour lines in the logarithmic diagram due to strong correlation of the corresponding parameters. Particularly the objective function calculated for different pre-exponential factors and activation energies (Fig. 8, right) shows an elongated valley that is unfavorable for parameter identification. Additionally, this finding emphasizes that the pre-exponential factor is more sensitive to perturbations than the activation energy or the exponent. An approach to improve the issue of correlated parameters in temperature dependent power law kinetics is given in [22, 23]. It was not applied here due to the different focus of the present study.

$$Error(S_k,T_m)=\frac{abs(K_{given}(S_k,T_m)-K_{est}(S_k,T_m))}{K_{given,\max}} \qquad \text{(eq. 22)}$$

$$Error_{average}=\frac{1}{n_S\cdot n_T}\sum_{k=1}^{n_S}\sum_{m=1}^{n_T}Error(S_k,T_m) \qquad \text{(eq. 23)}$$

for K = G, B_0, D (eq. 10); $S_k = S_{min}...S_{max}$ and $T_m = T_{min}...T_{max}$.

Nevertheless, the deviation (eq. 22) between the estimated and the given kinetic parameters is rather small as shown in figure 9. The depicted errors are 0.04% for growth, 0.1% for nucleation and 0.16% for dissolution on average (eq. 23). Thus, kinetic parameters can be re-estimated applying the short-cut-method via this optimization procedure. Furthermore, the information extracted from the CSD was fitted to every mechanism separately. Thus, the objective function does not depend on the solution of a full population balance model. Only the nonlinear correlations in the equations 19-21 are applied, which decreases the computational effort during the parameter estimation significantly.

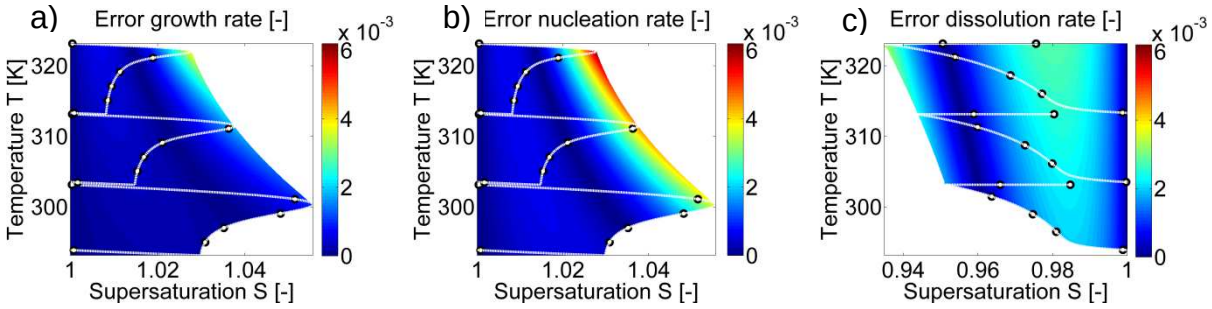

Fig. 9: Deviations (eq. 22) between the estimated and the pre-specified kinetics. a): Growth; *b):* Nucleation; *c):* Dissolution; *White dashed lines:* Transient temperature and supersaturation of the experiments used (compare Fig. 4); *Points:* Sample times of the solid phase.

4.1. Sub-model reduction

In the previous section, the ideal case was considered, where the structure of the "correct" rate laws is known (eq. 10). Commonly however, the kinetic mechanisms are unknown, when real experimental data are processed. In order to evaluate the magnitude of resulting errors, which occurs when a non-adequate kinetic law is assumed, the rate law given by equation 10 is simplified and applied to analyze the same *in silico* data as applied in the previous section. Thereby, the number of free parameters is reduced and thus, the complexity of the estimation problem is decreased. Two simplifications are chosen as examples. In the first scenario, a linear supersaturation dependence is assumed (p_3=1, eq. 24). In the second very simple scenario additionally temperature independent kinetics are assumed (p_2=0, p_3=1, eq. 25). Other scenarios are also possible but are not considered here.

$$K = p_1 \exp(\frac{-p_2}{RT})(S-1) \qquad \text{for K = G, D, } B_0 \qquad \text{(eq. 24)}$$

$$K = p_1 (S-1) \qquad \text{for K = G, D, } B_0 \qquad \text{(eq. 25)}$$

The two simplified kinetic sub-models (eq. 24 & 25) were applied to analyze the same synthetic data of the three experiments assuming again that five samples were taken. The errors in the quantified rates for the estimated kinetics with two free parameters (eq. 24) and one free parameter (eq. 25) are shown in figures 11 a)-c) and figures 11 d)-f), respectively. The errors increase with lowering the complexity of the kinetic approach as expected (compare Fig. 11 a) & d)). The deviations are particularly high, when the kinetics is rather fast as well as at the borders of the considered supersaturation and temperature ranges. Furthermore, the error of the dissolution kinetics is rather low compared to the errors of the nucleation and growth kinetics for both simplifications considered (eq. 24 & 25, table 5). This can be explained by the low supersaturation and temperature dependence of the original dissolution kinetic.

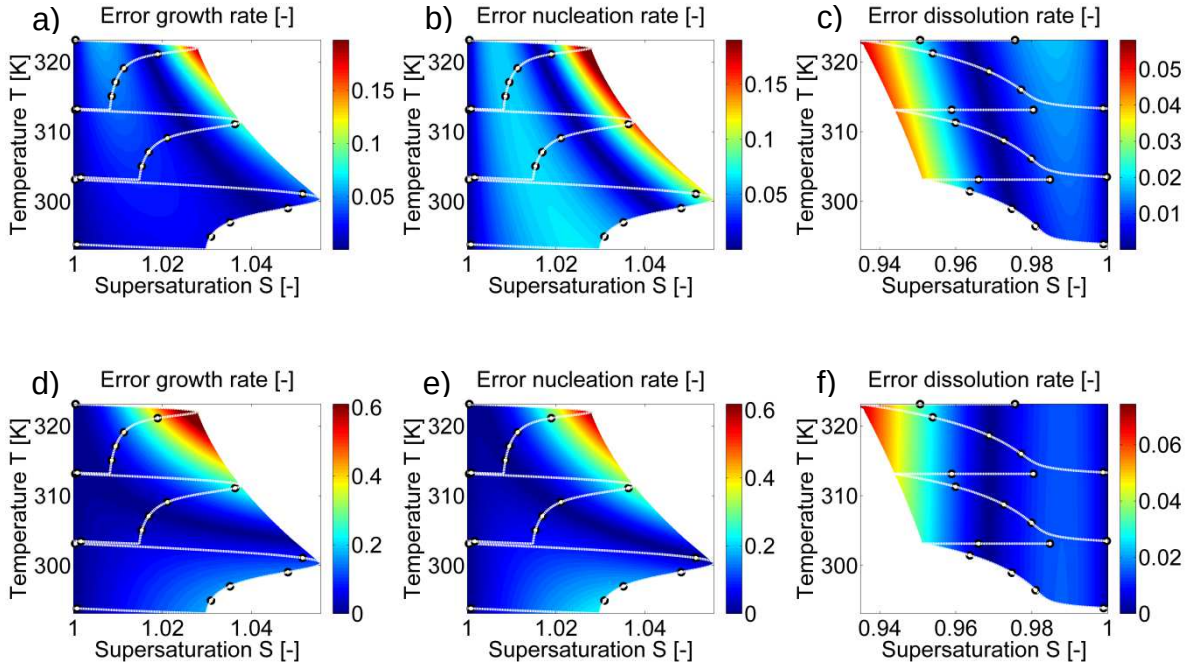

Fig. 10: Deviations (eq. 22) between the estimated kinetics with two free parameters (eq. 24 and parameters in table 5) and the given kinetics. *a):* Growth; *b):* Nucleation; *c):* Dissolution; Deviations (eq. 22) between the estimated kinetics with one free parameters (eq. 25 and parameters in table 5) and the given kinetics. *d):* Growth; *e):* Nucleation; *f):* Dissolution; *White dashed lines:* Transient temperature and supersaturation of the experiments used; *Points:* Sample times of the solid phase or times where CSD information is available for the parameter estimation.

The same holds for the average deviation (eq. 23) of the simplified estimated kinetics. The average error (compare table 4 and table 5) increases by a factor of 10 for dissolution if the supersaturation dependency is less pronounced (eq. 24) and by a factor of 50 to 70 for growth and nucleation. If additionally the temperature dependence is neglected as well (eq. 25), the average error doubles again for the latter two kinetic rates. Consequently, the deviation of the dissolution remains nearly constant as the temperature dependence is rather low (see table 2 for comparison).

Table 5: Values of the estimated kinetic parameters (eqs. 24, 25) and the corresponding average errors (eq. 23) for growth, nucleation and dissolution with a linear temperature dependent and independent kinetic approach. The data of three experiments, where five samples were taken, was applied. p_1 - pre-exponential factor; p_2 - activation energy; p_3 - exponent.

Kinetic	free parameters	p_1 [m/s; 1/s]	p_2 [J/mol]	p_3 [-]	$Error_{average}$ [%] (eq. 23)
Growth G	2	6.0×10^{5}	61.4×10^{3}	1	2.9
Nucleation B_0	2	1.9×10^{12}	32.7×10^{3}	1	5.3
Dissolution D	2	6.8×10^{-6}	1.3×10^{3}	1	1.4
Growth G	1	1.9×10^{-6}	0	1	10.2
Nucleation B_0	1	4.9×10^{5}	0	1	10.1
Dissolution D	1	4.1×10^{-6}	0	1	1.5

Even though an average error of 10% for the most simple linear rate law (eq. 25) is rather low, a fair evaluation is only possible if the kinetic rates themselves are compared to the considered supersaturation and temperature ranges.

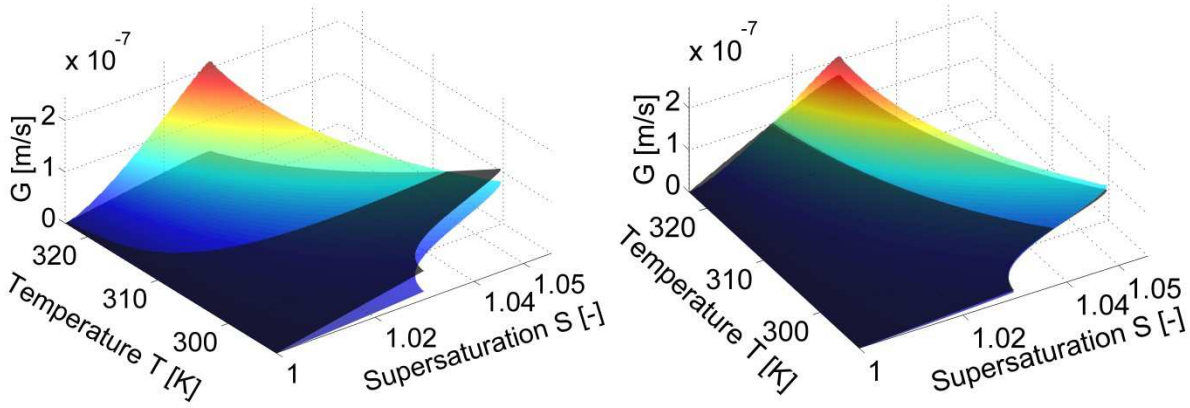

Fig. 11: Comparison of growth rates for different supersaturation and different temperature. *Left:* Comparison of the given kinetic (colored surface) with the estimated kinetic containing one free parameters (eq. 25, black surface). *Right:* Comparison of the given kinetic (colored surface) with the estimated kinetic containing two free parameters (eq. 24, black surface).

Figure 11 (left) shows that the linear kinetics intersects on a single curve with the original growth kinetics and strongly deviates otherwise. In contrary, a good description is achieved if the temperature dependence is conserved (eq. 24; Fig. 11, right). Hence,

a model prediction with this simplified kinetic approach would also agree rather well with experimental measurements.
In the following, to mimic unavoidable errors in the experimental data, the accuracy of the proposed short-cut-method is investigated by evaluating measurement signals that exhibit deviations from the perfect *in silico* data.

4.2. Influence of measurement error

In contrast to simulated (i.e. *in silico*) data, experimental measurements have limited precision, e.g. for the determination of the solubility curve and the resulting supersaturation level. Several distortions or errors occur due to manual mistakes during the experimental procedure, the accuracy of measurement technology or random deviations. Hence, the results of the data analysis and processing will be erroneous as well. Therefore, the error propagation for the presented short-cut-method has to be investigated. At first the amount of samples and experiments is kept constant but two different noisy measurements are assumed.
Essential for the estimation scheme are the information of the CSD as well as the concentration and temperature levels of the liquid phase. The precision of the entire particle size distribution is strongly dependent on the applied measurement technique. For example, the correct amount of very small particles is hardly detectable by a sieve analysis. On the other hand, reflections and scattering of big crystals will influence the accuracy of laser diffraction measurement techniques. A general and precise simulation of these errors is impossible. Thus, a generic error will be assumed for both required information of the CSD, the crystal number and the mean length evolution of the seed fraction. The transient data point will be distorted randomly with a maximal deviation of 5% of the actual value (Fig. 12, left).
Another important information for kinetic estimation methods is the super- or undersaturation. Here, the precision of the concentration measurement and the accuracy of the solubility curve are decisive. Therefore, a stochastic error is assumed for the concentration and the temperature information for the solubility data points depicted in figure 2. Subsequently, a new solubility curve (eq. 14) was fitted to the faulty data and applied for the parameter estimation. A maximal stochastic error of 1% was assumed for the solubility analysis based on own experience. Furthermore, a noise level of 1% was applied to the concentration signal. An example for the resulting distorted supersaturation signal is depicted in figure 12 (left).
It can be expected that also an error of the temperature information influences the subsequently estimated kinetic rates. However, resistance temperature measurement devices are quite precise and the impact should be rather small in comparison to the other defective signals considered. Therefore, this case is not investigated in the present study.

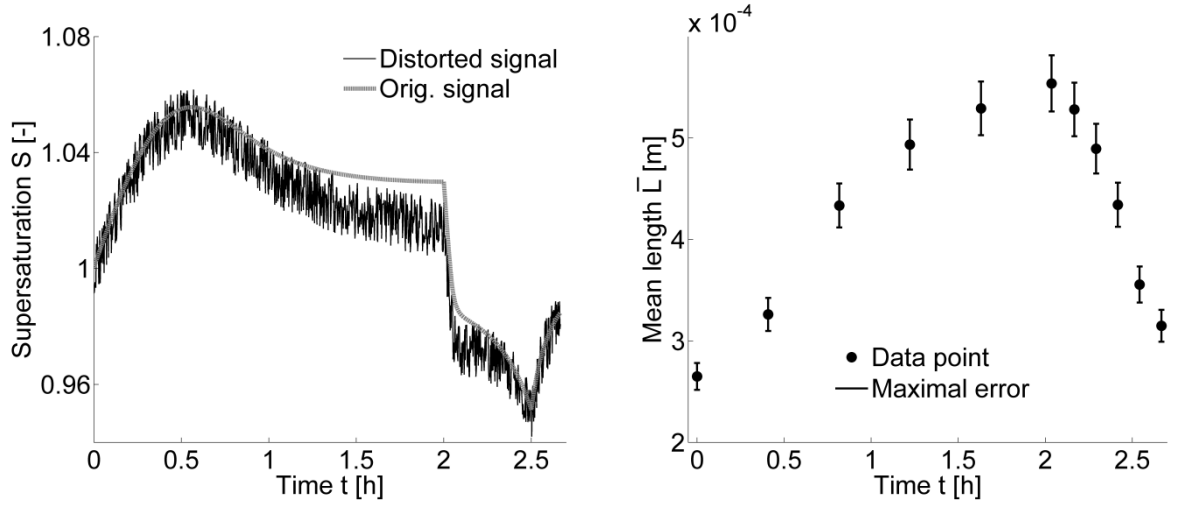

Fig. 12: Example of randomly distorted measurement signals. *Left:* Supersaturation signal, which was created by a stochastic fluctuation of the concentration signal in combination with a deflected saturation curve. *Right:* Mean length of the seed fraction of the simulated experiment 1. The black lines depict the maximum error, which was randomly added to the original data.

It should be noted, that the assumed stochastic errors do not cover all effects which can occur in wet-lab experiments. Nevertheless, they serve as an example to investigate how robust the short-cut-method for different kinetic sub-models (eqs. 10, 24, 25) is. All parameters of all models were estimated 10 times for different erroneous measurement information. The mean of the average errors (eq. 23) with respect to the original kinetics are shown together with the corresponding standard deviation in figure 13.

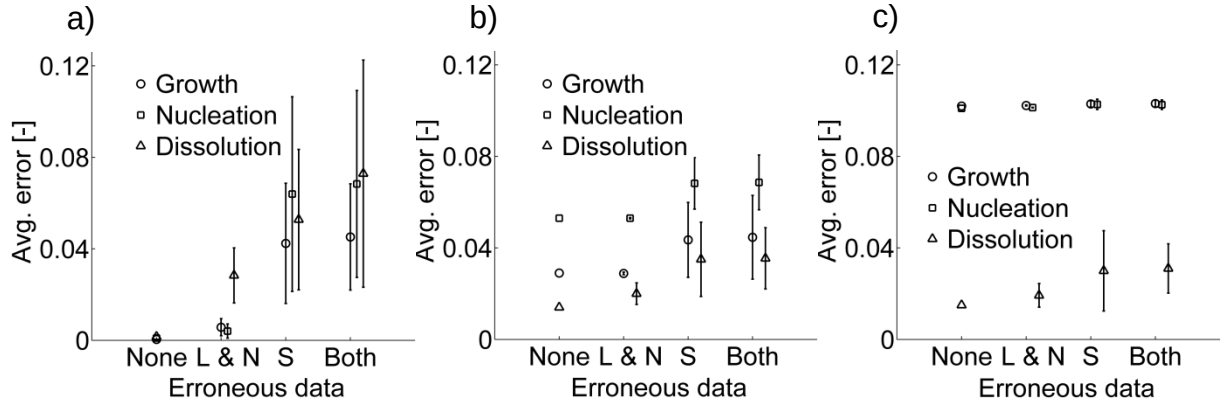

Fig. 13: Resulting average kinetic errors of the three kinetic phenomena calculated according to eq. 23 for different distorted measurement signals. The kinetic parameters were estimated applying the short-cut-method together with the original signal ("None"), the distorted seed mean length and crystal number ("L & N"), the erroneous supersaturation signal ("S") or both errors ("Both"). *a)*: Average errors for all three estimated kinetics applying an approach with three free parameters (eq. 10). *b)*: Average errors for all three estimated kinetics applying an approach with two free parameters (eq. 24). *c)*: Average errors for all three estimated kinetics applying an approach with one free parameter (eq. 25). The error bars depict the standard deviation of 10 different estimates with randomly generated distorted signals.

It can be seen that the identification of the correct kinetic model parameters (eq. 10, Fig. 13 a) is quite sensitive to measurement errors. Furthermore, it can be concluded that a noisy supersaturation signal (“S”) has a higher impact compared to noise applied to the crystal length and number information (“L & N”). An exception is the average error of the dissolution kinetics that is rather sensitive towards deviations in the evolution of the mean lengths of the seed fraction. It can be supposed that the stronger dynamic of the data is one reason for this fact since the dissolution is rather fast compared to nucleation or growth. Furthermore, this relation can be found also for the other model approaches. If the supersaturation signal and the crystal length and number information are erroneous (Erroneous signal “Both”) for the parameter estimation a simple superimposition of the single errors can be observed.
The trends described for the model approach with three free parameters become apparent for the other model approaches as well (Fig. 13 b) and c). Nevertheless, a decreasing amount of free parameters, which have to be estimated, leads to higher robustness if measurement errors occur. For example, the kinetic approach with two free parameters (eq. 24, Fig. 13 b) has lower average kinetic errors and lower standard deviations if noise is applied to both measurement signals.
In contrary, almost no change is observed for the growth and nucleation kinetics with one free parameter (eq. 25, Fig. 13 c). The initial kinetics cannot be described by a linear approach and thus, measurement errors will have a rather low influence the error propagation in this case. The dissolution kinetics can be reflected by a linear approach since it has a rather low supersaturation and temperature dependence. Thus, the effect of erroneous measurement signals is visible in that case.
The mean parameters, which were estimated with the defective transient measurement signals, are listed in table 6 together with the estimated parameters applying the original signals for all three model approaches. It can be seen that none of the parameters can be re-estimated exactly except the kinetic approach with one single free parameter. The reason is the correlation of the corresponding parameters of the applied power laws (eqs. 10 and 24). Hence, erroneous measurement information induces a strong shift of the global minimum of the objective function and therefore completely different parameter combinations. Furthermore, local minima, which can occur due to the randomized errors, have to be taken into account. Hence, the high standard deviation especially of the pre-exponential factor is obvious.

Table 6: Estimated kinetic parameters for growth, G, nucleation, B, and dissolution, D, rate. The mean values of the parameters of the three different considered approaches (eqs. 10, 24, 25) are given, which were estimated applying the perfect (Orig.) and the distorted (Error) measurement signals. p_1 - pre-exponential factor; p_2 - activation energy; p_3 - exponent; σ - absolute standard deviation.

Free parameter	Kinetic	Signal	$p_{1,mean}$ [m/s; 1/s]	$\pm\sigma$	$p_{2,mean}$ [J/mol]	$\pm\sigma$	$p_{3,mean}$ [-]	$\pm\sigma$
3	G	Orig.*	$5x10^{7}$		$75x10^{3}$		1.4	
		Error	$2.1x10^{8}$	$6.6x10^{8}$	$62.7x10^{3}$	$9x10^{3}$	1.2	0.4
	B	Orig.*	$1x10^{15}$		$50x10^{3}$		1.5	
		Error	$2.9x10^{13}$	$4.8x10^{13}$	$31.8x10^{3}$	$8.8x10^{3}$	1.2	0.5
	D	Orig.*	$6x10^{-6}$		100		1.1	
		Error	$1.9x10^{-4}$	$3.3x10^{-4}$	$7.3x10^{3}$	$5.9x10^{3}$	0.8	0.3
2	G	Orig.**	$6x10^{5}$		$61.4x10^{3}$			
		Error	$1.3x10^{10}$	$4x10^{10}$	$58.7x10^{3}$	$14.9x10^{3}$		
	B	Orig.**	$1.9x10^{12}$		$32.7x10^{3}$			
		Error	$9.1x10^{13}$	$2.9x10^{14}$	$27.3x10^{3}$	$10.1x10^{3}$		
	D	Orig.**	$6.8x10^{-6}$		$1.3x10^{3}$			
		Error	$2.1x10^{-4}$	$3.1x10^{-4}$	$5.8x10^{3}$	$5.7x10^{3}$		
1	G	Orig.**	$1.9x10^{-6}$					
		Error	$1.9x10^{-6}$	$1.5x10^{-7}$				
	B	Orig.**	$4.9x10^{5}$					
		Error	$4.9x10^{5}$	$3.8x10^{4}$				
	D	Orig.**	$4.1x10^{-6}$					
		Error	$4.2x10^{-6}$	$4x10^{-7}$				

* compare table 2
** compare table 5

However, a higher accuracy of the estimated kinetic rates can be expected if more information is provided for the short-cut-method. Hence, the impact of the amount of experiments and CSD samples must be investigated as well. Therefore, the evolution of the average error (eq. 23) between the given and the estimated kinetic is investigated with respect to an increasing amount of experimental data. Figure 14 a) shows, that at least three experiments and three CSD samples are necessary for a kinetic approach with three free parameters (eq. 10) to achieve a low average error. However, a further increase of CSD samples does not necessarily result in a better estimate. It can be seen that even with 12 CSD samples a worse estimate is possible compared to the case where four CSD samples are applied.
Regarding this fact, there is evidence that four samples of one single experiment is in general not sufficient for the estimation of kinetic rates as suggested by Yokota et al. [11], if the precision of the measured quantities is not high enough.
In contrast, a kinetic approach with two free parameters (Fig. 14 b) shows already a good fit if only two experiments and at least two CSD samples are provided.

Furthermore, the kinetic approach with one free parameter (Fig. 14 c)) will not give a much better result regardless how much information is provided.
It should be mentioned, that the conclusions drawn above are distinct for the specific randomized errors considered. The results will differ significantly if, e.g. static or oscillating errors, are considered as well.

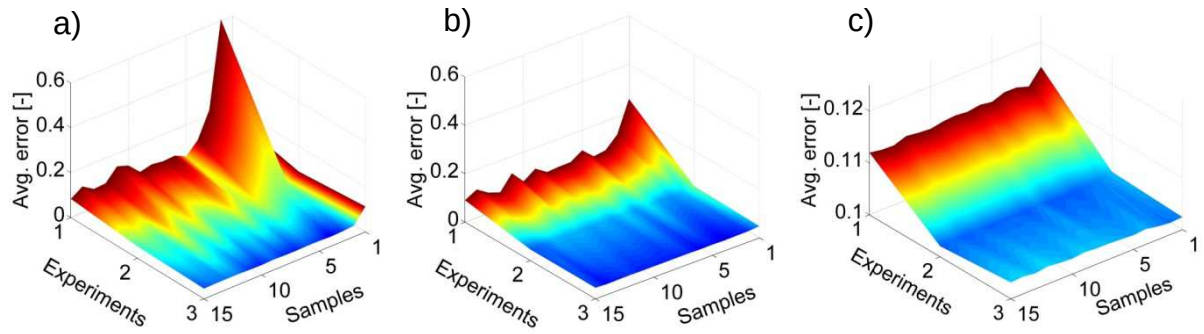

Fig. 14: Average deviations (eq. 23) between the estimated growth kinetics and the given kinetics applying different sub-models and different amounts of experiments and CSD samples. *a):* Estimated growth approach with 3 free parameters (eq. 10); *b):* Estimated growth approach with 2 free parameters (eq. 24); *c):* Estimated growth approach with 1 free parameter (eq. 25).

The concept of the short-cut-method is to apply the least amount of experiments and CSD samples to reduce the effort for the quantification of kinetic rates. However, a general conclusion cannot be stated since the necessary amount of experimental information depends on the complexity of the original kinetics, the precision of the measurement devices and the amount of model parameters to be determined. For the specific constellation considered it can be stated that two experiments with three CSD samples are sufficient to determine the parameters of the growth, nucleation and dissolution kinetic if a model with two free parameters is assumed. This yields an average error of 5% with respect to the original kinetics and the considered range of supersaturation and temperature (eq. 23).
However, in general the average deviations and the precision of the parameters are not of major interest. Crucial for the short-cut-method is the efficient quantification of kinetic rates to optimize existent or design new crystallization processes. Hence, the effect of the discussed deviations is evaluated with respect to the performance of a simulated crystallization process in the next section.

5. Application of the prediction method and design of a continuous crystallization process

To evaluate the quality of the initially assumed parameters and the parameters estimated utilizing the short-cut method, they are used in this section to predict another industrially relevant type of crystallization process. Therefore, a mixed-suspension, mixed-product-removal (MSMPR) process is considered. It can be assumed, that deviations from the original kinetics will have a larger impact on the process results compared to the batch case due to the continuous operation.
The batch crystallizer model introduced in chapter 2 (eqs. 2 and 4) is modified to describe the continuous crystallization process (eqs. 26 and 27). The well-known model [12] additionally assumes a non-classifying product withdrawal and a crystal-free inlet stream. All other assumptions and conditions, e.g. the initial seeding, are identical to the batch crystallizer model.

$$\frac{\partial f(t,L)}{\partial t} = -G(S(t),T(t))\frac{\partial f(t,L)}{\partial L} - \frac{f(t,L)}{\tau} \qquad \text{(eq. 26)}$$

$$\frac{dc(t)}{dt} = \frac{1}{\tau}\left(\frac{\rho_{solvent,in}}{\rho_{solvent}} c_{in} - c(t)\right) - \frac{3k_v \rho_{solid} G(S(t),T(t))}{V_{solvent}\rho_{solvent}} \int_{L\min}^{L\max} L^2 f(t,L)dL \qquad \text{(eq. 27)}$$

$$\frac{1}{\tau} = \frac{\dot{V}}{V_{Reactor}} \qquad \text{(eq. 28)}$$

If the original kinetics for growth and nucleation (Table 2) are applied, the product quality, e.g. the mean size (eq. 15), and the outlet concentration can be calculated for various combinations of supersaturation, S, temperature, T, and mean residence time, τ (eq. 28). Figure 15 illustrates these calculations with respect to the mean product crystal size. The bold black lines depict in the τ-S-plane the mean product levels for the considered supersaturations and mean residence times at constant temperature. Whereas, the S-T-plane depicts the mean product levels for the considered supersaturation and temperatures at constant mean residence time. It can be seen for the considered range of the process variables, that the influence of the crystallization temperature is higher than the effect of supersaturation and the mean residence time due to the strong temperature dependency of the growth and nucleation kinetics. Furthermore, smooth curves result for the contours of the product quality for the simple power-law kinetics chosen.
Additionally, if the total crystal mass inside the reactor drops below the initial seed mass no steady-state is achievable as the crystallizer would run out of solid material. This assumption is necessary since secondary nucleation yields positive values independent of the process conditions. Thus, even if the mean residence time approaches zero and the supersaturation approaches one, a continuous crystallization would be possible, which is not feasible.
Three different combinations of temperature, supersaturation and mean residence time were chosen leading to different steady-states, which serve for the comparison (Table

7, black dots in Fig. 15). Considering the trajectories of the batch experiments (Fig. 15 right) these combinations are in the range of the observed supersaturation and temperature. Nevertheless, for point two and three the highest deviations are expected as they are near the border where the estimated kinetics is assumed to be valid. For every combination of process parameters, the continuous crystallization was simulated for a span of 10 mean residence times. This ensures steady state operation that was reached after 5-8 mean residence times for the applied conditions. Subsequently, the model approaches with three, two and one free parameters (eqs. 10, 24, 25) is applied and the mean product sizes as well as the outlet supersaturation are compared to the original kinetics. It should be mentioned, that the different parameter combinations resulting from the 10 randomly erroneous supersaturation and CSD information are applied and not their mean values (Table 6).

Table 7: Tested process variables combinations of the different steady-states.

	T [K]	S [-]	τ [h]
P1	300	1.027	0.42
P2	300	1.053	0.83
P3	322	1.027	0.83

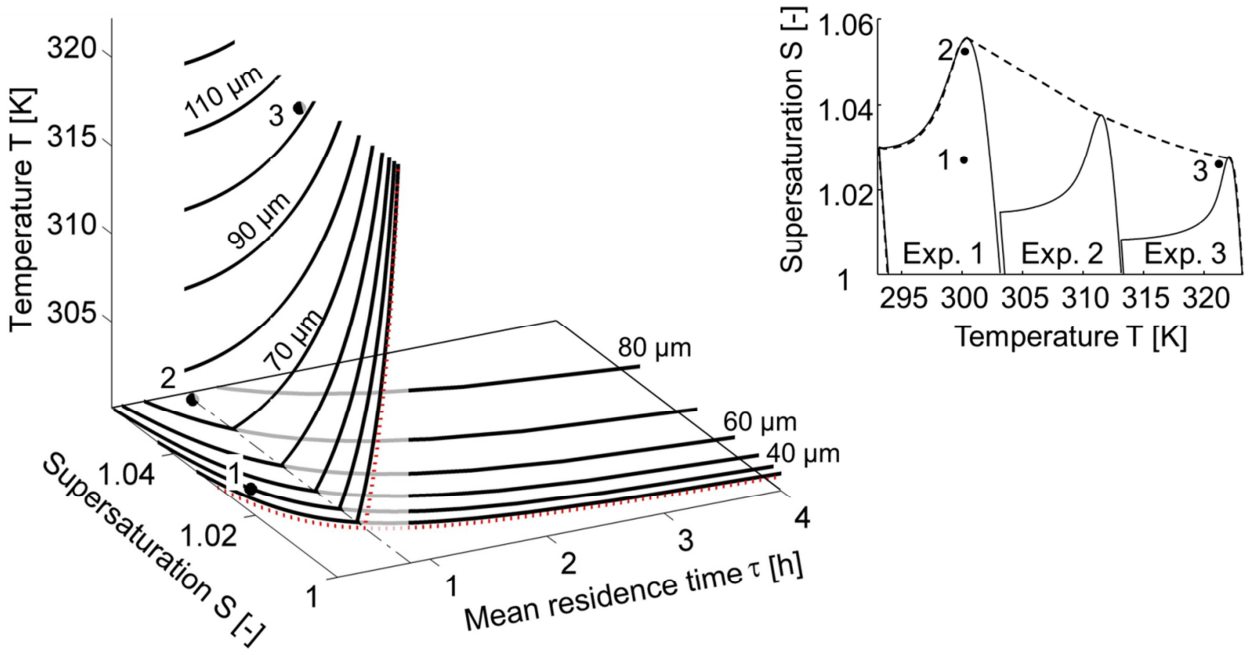

Fig. 15 *Left*: Mean product size (eq. 15) of a continuous crystallization process applying the original kinetic parameters and the kinetic law of eq. 10. *Bold black lines:* Contour lines of the mean product size with some indicated values. *Red dashed line:* Assumed border of achievable steady-states with respect to the process variables. *Right*: Tested process parameter combinations for the evaluation of the quality of the kinetics in context with the trajectories of the simulated batch experiments. *Points:* Indications of tested process parameter combinations for the evaluation of the quality of the kinetics, which were estimated applying distorted measurement signals.

Table 8 shows the results of the continuous crystallization simulations for the three operating conditions and the different models. The comparison between the original and the estimated kinetics shows that the outlet supersaturation and the mean product size are well predictable with the model approaches consisting of two and three free parameters (eqs. 10, 24). The differences of the mean crystal size (product quality) are 3.9% and 1.8% on average. Furthermore, the predictions of the final supersaturation and solute concentration (not shown in table 8) exhibit an average error of 0.1%. Thus, the estimated kinetic parameters are applicable to predict and analyze the considered continuous crystallization process even though the parameter estimation was done with faulty measurement signals. The linear model approach deviates the most with around 1% regarding the outlet supersaturation and with nearly 25% with respect to the product mean size. In summary, all kinetic approaches are able to predict the final liquid composition of the steady-states rather precisely. With respect to the product quality deviations are higher using the linear approach, but much lower with the more complex models.

Table 8: Results of the continuous crystallization process simulation for three different combinations of process variables. Depicted are the mean supersaturation and the mean product size (eq. 15) from the steady-state using the original and the estimated kinetics, which were optimized (eqs. 10, 24, 25) with different distorted measurement signals (compare Table 6). σ - Absolute standard deviation.

Set point	Free parameter (eq.)	S_{end}	±σ [-]	μ_{end} [µm]	±σ [µm]
P1	Orig.	1.025		39.5	
	3 (eq. 10)	1.024	0.002	40.8	7.8
	2 (eq. 24)	1.024	0.001	43.8	3.6
	1 (eq. 25)	1.019	0.001	57.5	1.7
P2	Orig.	1.025		76.1	
	3 (eq. 10)	1.023	0.006	75.9	3.6
	2 (eq. 24)	1.021	0.002	76.8	2.7
	1 (eq. 25)	1.015	0.001	86.2	0.1
P3	Orig.	1.008		102.2	
	3 (eq. 10)	1.008	0.003	100.1	4.7
	2 (eq. 24)	1.006	0.001	102.9	3.3
	1 (eq. 25)	1.014	0.001	80.6	1.5

6. Conclusion

In summary, the presented short-cut-method is capable of quantifying growth, nucleation and dissolution rates for the here presented systems. It could be shown that a sporadic sampling of the solid phase is sufficient to follow the evolution of the crystal phase with respect to the total number and the enlargement of the seed crystal fraction. In the following, the original kinetic parameters were re-estimated with this sparse information at high precision.
The required flow of information of the short-cut-method is illustrated in figure 16.

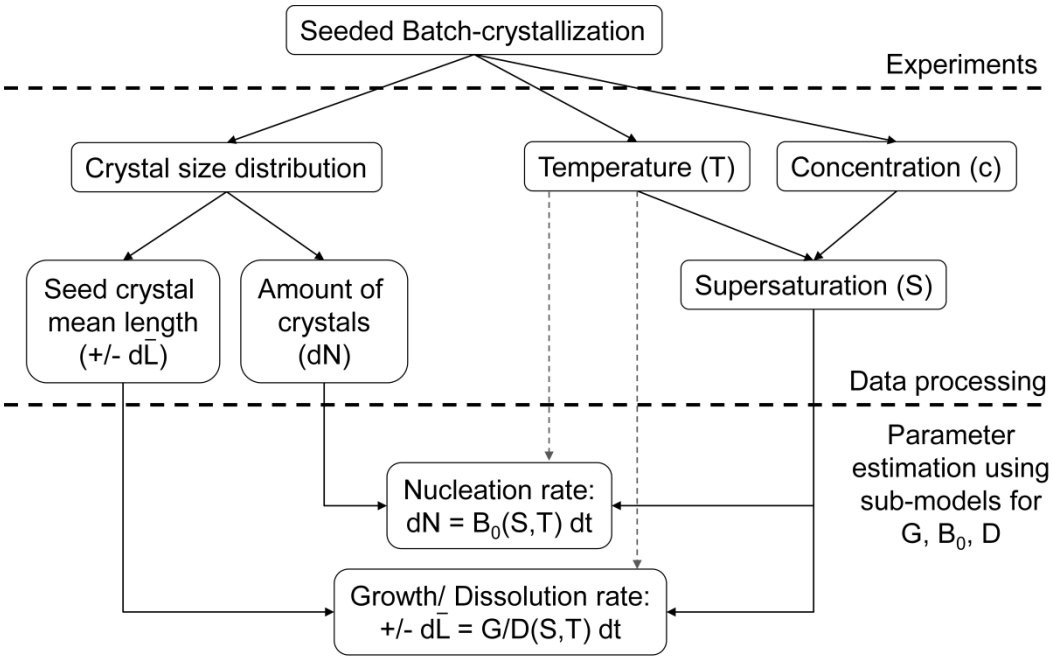

Fig. 16: Scheme of the proposed short-cut method.

The sampled crystal size distributions from the seeded batch experiments are analyzed regarding the grown seed fraction and the total particle number. These data serve as the experimental input values for the subsequent quantification of the rate law parameters. The super- or undersaturation is calculated based on the solubility curve together with the corresponding temperature and concentration signal. Finally, appropriate sub-models are chosen to calculate theoretical rates with the data of the liquid phase and the comprised parameters are estimated by comparison with the experimental information.
However, the correct kinetic approaches and their complexity are usually unknown for new substances and thus simplifications of the initial kinetics are compared in this work. It can be stated that a simplification of the kinetic law is justified if the main dependencies are conserved. An oversimplification will lead to rather high uncertainties of the model predictions. But several kinetic models can be evaluated efficiently with the here proposed short-cut-method since the computational effort of the estimation routine is rather low.

Afterwards, the synthetic data was distorted randomly to simulate measurement errors as well as to quantify the error propagation for the estimation procedure. It was found that a precise supersaturation signal is most important to achieve a correct fit of the kinetics. Furthermore, it could be shown that the more complex model approach was rather sensitive to erroneous input signals. Eventually, if all measurement errors were considered together, the models with two and three free parameters exhibited the same quality.
Furthermore, the data amount, which is provided for the optimization routine, is also decisive for the resulting accuracy if erroneous measurement signals are involved. It was shown, that for the considered situation at least three experiments for the model approach with three free parameters and two experiments for the model approach with two free parameters together with three CSD samples are necessary to achieve a good estimation result.
A continuous crystallization process was analyzed with the different sets of estimated parameters since the main focus of the short-cut-method is to efficiently evaluate crystallization process performances. Three different process variable combinations, which led to three different steady-states, were chosen to evaluate the quality of the estimated kinetic rates in case of faulty measurement signals. Even though, the estimated kinetics with three and two free parameters deviated from the original kinetics on average by 8%, the deviation from the expected steady-state condition was only 0.1% with respect to the liquid phase and 3-4% with respect to the product quality. This is only one possible application where the short-cut-method serves for parameterizing the overall process model. Generally, the proposed method can be applied to every crystallization processes described by one internal coordinate (e.g. particle size). It should be emphasized, that the seed population serves as a benchmark for the whole crystal ensemble. A different growth behavior due to growth rate dispersion e.g. exposed by nucleated particles will not be detected. Furthermore, the characteristic length of the particles is among other things mainly defined by the CSD measurement technique. A Laser diffraction measurement of a certain crystal population yields a different size distribution than e.g. sieve analysis. Hence, the kinetic investigations have to be carried out with one and the same method with the characteristic length defined by the measurement principle.
The proposed short-cut-method is capable of estimating and quantifying rates with various kinetic model approaches. Furthermore, it provides reliable kinetic parameters, which can be validated with corresponding *in silico* experiments. Additionally, the numerical effort is reduced because every kinetic approach is estimated separately and there is no need to use the population balance model. The experimental proof of this procedure is the task of a second paper.

Acknowledgements

Andreas Seidel-Morgenstern and Kai Sundmacher gratefully acknowledge the support of this research work by the German Research Foundation (DFG) under the grants SE 586/ 20-2 and SU 189/6-2 respectively, embedded in the Priority Programme SPP 1679.

Symbols & abbreviations

Avg. error	[-]	Average error
abs	[-]	Absolute value
B_0	[1/s]	Nucleation rate
b	[-]	Nucleation exponent
c	[-]	Concentration (mass loading, $g_{Solute}/g_{Solvent}$)
D	[m/s]	Dissolution rate
d	[-]	Dissolution exponent
$E_{A,i}$	[J/Kmol]	Activation energy for the diff. kinetic approaches (i = g, b, d)
Error	[-]	Error
f	[#/m]	Number density distribution/ function
G	[m/s]	Growth rate
g	[-]	Growth exponent
i	[-]	Exponent of the Arrhenius approach (i = g, b, d)
K	[m/s; 1/s]	Kinetic G, B_0 or D
k_V	[-]	Volume shape factor
k_i	[m/s; 1/s]	Rate constant for i = g, b, d
L	[m]	Property coordinate
$\bar{L}$	[m]	Mean length
$\log_{10}$	[-]	Logarithm to the base 10
m	[kg]	Mass
N	[#/m^3]	Crystal number
n	[-]	Number in eq. 23
OF	[m; #]	Objective function
p	[-]	Parameters for the solubility correlation and kinetic laws
R	[J/Kmol]	Universal gas constant
ρ	[kg/m^3]	Density
S	[-]	Relative Supersaturation
σ	[m]	Standard deviation
T	[K]	Temperature
t	[h]	Time
τ	[h]	Mean residence time
θ	[°C]	Temperature
V	[m^3]	Volume
$\dot{V}$	[m^3/h]	Volumetric flow rate

Sub- & Superscripts

Average	Average
End	Final
Est	Estimated
Exp	Experiment
In	Inlet stream
Liquid	Liquid phase

Max	Maximum value
Mean	Mean value
Min	Minimum value
Reactor	Reactor
Sample	Sample
Sat	Saturation
Seed	Seed
Sim	Simulated
Solid	Solid phase
Solvent	Solvent
0	Initial value
*	Saturation

References

[1] Beckmann, W. (ed.); *Crystallization - Basic Concepts and Industrial Applications*, Wiley-VCH, Weinheim, 2013, Vol. 1, Chapter 1, pp 1-7.

[2] Mersmann, A.; Braun, B.; Loeffelmann, M. *Chem. Eng. Sci.*, 2002, 57, 4267-4275.

[3] Garside, J.; Mersmann. A.; Nývlt, J.; *Measurement of Crystal Growth Rates*, European Federation of Chemical Engineering, Working Party on Crystallization, Germany, 1990, Vol. 1.

[4] Borchert, C.; Temmel, E.; Eisenschmidt, H.; Lorenz, H.; Seidel-Morgenstern, A.; Sundmacher, K. *Cryst. Growth Des.*, 2014, 14, 952-971.

[5] Mahoney, A. W.; Doyle, F. J.; Ramkrishna, D. *AIChE J.*, 2002, 48, 981-990.

[6] Ulrich, J.; *Kristallwachstumsgeschwindigkeiten bei der Kornkristallisation*, professorial dissertation, Bremen, 1989.

[7] Temmel, E.; Lorenz, H.; Seidel-Morgenstern, A. In *ISIC 19th, International Symposium on Industrial Crystallization*, Book of Abstracts, Toulouse, France, 2014, 548-550.

[8] Gutwald, T; *Über die Bestimmung kinetischer Parameter bei der diskontinuierlichen Kristallisation aus Lösungen*, Dissertation, Technical University Munich, Munich, 1991.

[9] O'Ciardha, C. T.; Hutton, K. W.; Mitchell N. A.; Frawley, P. J. *Cryst. Growth Des.*, 2012, 12, 5247-5261.

[10] Kessler, W. (ed.); *Prozessanalytik,* Wiley-VCH, Weinheim, 2006, Vol. 1.

[11] Yokota, M.; Sato, N.; Kubota, N. *Chem. Eng. Sci.*, 2000, 55, 717-722.

[12] Randolph A. D.; Larson, M. A.; *Theory of particulate processes - Analysis and Techniques of Continuous Crystallization*, Academic Press Inc., London, 1988, Vol. 2.

[13] Mullin, J. W.; *Crystallization*, Butterworth-Heinemann, Boston, 1997, Vol. 3.

[14] Versteeg, H. K.; Malalasekera, W.; *An Introduction to computational fluid dynamics*, Longman Scientific & Technical, New York, 1995, Vol. 1.

[15] Dormand, J. R.; Prince P. J. *J. Comput. Appl. Math.*, 1980, 6, 19-26.

[16] Karpinski, P.; Nývlt, J. *Cryst. Res. Technol.*, 1982, 17, 383-388.

[17] Mohan, R.; Myerson, A. S. *Chem. Eng. Sci.*, 2002, 57, 4277-4285.

[18] Zhang, F.; Mangold, M.; Kienle, A. *Chem. Eng. Technol.*, 2009, 32, 641-649.
[19] Kiedorf, G.; Hoang, D.M.; Müller, A.; Jörke, A.; Markert, J.; Arellano-Garcia, H.; Seidel-Morgenstern, A.; Hamel, C. *Chem. Eng. Sci.*, 2014, 115, 31-48.
[20] Jörke, A.; Triemer, S.; Seidel-Morgenstern, A.; Hamel, C. *Chem. Ing. Tech.*, 2015, 87, 713-725.
[21] Lagarias, J.C.; Reeds, J. A.; Wright, M. H.; Wright, P. E. *SIAM J. Optim.*, 1998, 9, 112-147.
[22] Schwaab, M.; Pinto, J. C. *Chem. Eng. Sci.*, 2007, 62, 2750-2764.
[23] Schwaab, M.; Lemos, L. P.; Pinto, J. C. *Chem. Eng. Sci.*, 2008, 63, 2895-2906.

For Table of Contents Use Only

Title:
A short-cut-method for the quantification of crystallization kinetics - Part 1: Method development

Authors:
Erik Temmel, Holger Eisenschmidt, Heike Lorenz, Kai Sundmacher, Andreas Seidel-Morgenstern

Synopsis:
A short-cut-method for the estimation of nucleation, growth and dissolution kinetics for 1-dimensional PBE models is developed. It is based on analyzing the evolution of the crystal size distribution during a few batch crystallization experiments to efficiently parameterize appropriate kinetic sub-models. The procedure, the error propagation as well as the applicability to crystallization processes are discussed theoretically.

TOC graphic